# Rotationally Resolved Absorption Cross Sections of Formaldehyde in the 28100−28500 $cm^{-1}$ (351−356 nm) Spectral Region: Implications for in Situ LIF Measurements

**Dick T. Co,* Thomas F. Hanisco, and James G. Anderson**

*Department of Chemistry and Chemical Biology, Harvard University, Cambridge, Massachusetts 02138*

**Frank N. Keutsch**

*Department of Chemistry, University of Wisconsin−Madison, Madison, Wisconsin 53706*

*Received: June 26, 2005; In Final Form: September 29, 2005*

The rotationally resolved ultraviolet absorption cross sections for the $2^0_0 4^1_0$ vibrational band of the $A^1A_2-X^1A_1$ electronic transition of formaldehyde (HCHO) at an apodized resolution of 0.027 $cm^{-1}$ (approximately 0.0003 nm at 352 nm) over the spectral range 28100−28500 $cm^{-1}$ (351−356 nm) at 298 and 220 K, using Fourier transform spectroscopy, are first reported here. Accurate rotationally resolved cross sections are important for the development of in situ HCHO laser-induced fluorescence (LIF) instruments and for atmospheric monitoring. Pressure dependence of the cross sections between 75 and 400 Torr at 298 K was explored, and an average pressure broadening coefficient in dry air of $1.8 \times 10^{-4}$ $cm^{-1}$ $Torr^{-1}$ for several isolated lines is reported. Gaseous HCHO was quantitatively introduced into a flow cell by evaporating micron-sized droplets of HCHO solution, using a novel microinjector technique. The condensed-phase concentrations of HCHO were determined by iodometric titrations to an accuracy of <1%. Accuracy of the measured absorption cross sections is estimated to be better than ±5%. Integrated and differential cross sections over the entire band at low resolution (~1 $cm^{-1}$) obtained with our calibration technique are in excellent agreement with previous measurements. A maximum differential cross section of $5.7 \times 10^{-19}$ $cm^2$ $molecule^{-1}$ was observed at high resolution—almost an order of magnitude greater than any previously reported data at low resolution.

## 1. Introduction

Formaldehyde (HCHO) is an important atmospheric compound and is critical to the understanding of the chemistry of hydrogen radicals ($HO_x = OH + HO_2$), nitrogen radicals ($NO_x = NO + NO_2$), and ozone ($O_3$) in the atmosphere. Hydrogen radicals are central to the photochemistry of the atmosphere[1] despite having mixing ratios of only a few parts per trillion by volume (pptv). In the stratosphere, the $HO_x$ radicals are important in the removal of $O_3$ through direct reaction with $O_3$ and the nitrogen and hydrogen chemical families and indirectly through reactions with the halogen oxides (ClO, BrO, and IO). In the troposphere, $O_3$ production is dominated by the catalytic cycle involving the oxidation of CO and other hydrocarbons by OH and rate limited by the oxidation of NO by $HO_2$ and $RO_2$. Because of the extensive coupling of $HO_x$ to these chemical families, understanding these mechanisms is important in understanding $O_3$ photochemistry, which has a broad societal impact on human health.

The primary source of $HO_x$ in the lower atmosphere is the oxidation of water vapor, hydrogen-containing source gases, and methane ($CH_4$) by excited-state oxygen atoms $O(^1D)$ produced from the photolysis of $O_3$. Though the $O(^1D) + H_2O \rightarrow 2OH$ reaction is the primary source of OH, the oxidation of $CH_4$ and other convectively transported hydrogen-containing species can be a significant source of $HO_x$ in the dry upper troposphere. The interest in formaldehyde lies in its role as a reaction intermediate in the oxidation of $CH_4$ initiated by reaction with $O(^1D)$ (and in similar sequences by reactions with OH and Cl):

$$O_3 + h\nu \rightarrow O(^1D) + O_2 \quad (1)$$

$$O(^1D) + CH_4 \rightarrow CH_3 + OH \quad (2)$$

$$CH_3 + O_2 + M \rightarrow CH_3O_2 + M \quad (3)$$

$$CH_3O_2 + NO \rightarrow CH_3O + NO_2 \quad (4)$$

$$NO_2 + h\nu \rightarrow NO + O \quad (5)$$

$$O + O_2 + M \rightarrow O_3 + M \quad (6)$$

$$CH_3O + O_2 \rightarrow HCHO + HO_2 \quad (7)$$

$$HCHO + h\nu \xrightarrow{\sim 1/3} H + CHO \quad (\lambda < 340 \text{ nm}) \quad (8)$$

$$CHO + O_2 \rightarrow HO_2 + CO \quad (9)$$

$$H + O_2 + M \rightarrow HO_2 + M \quad (10)$$

$$\text{Net: } CH_4 + 4O_2 \rightarrow OH + 3HO_2 + CO$$

where each $CH_4$ consumed can produce as many as four $HO_x$. $HO_x$ concentrations are also maintained by the autocatalytic oxidation of hydrocarbons, e.g., methane, initiated by OH. Even though OH is first consumed at the initiation step

$$OH + CH_4 \rightarrow CH_3 + H_2O \quad (11)$$

Reactions 3−10 can return as many as three $HO_x$. An alternate

* Address correspondence to this author. E-mail: co@huarp.harvard.edu.

10.1021/jp053466i CCC: $30.25 
Published on Web 11/05/2005

pathway for the photolysis of HCHO in reaction 8 is the production of $H_2$ and CO:[2]

$$\mathrm{HCHO} + h\nu \xrightarrow{\sim 2/3} \mathrm{H_2} + \mathrm{CO} \qquad (\lambda < 365\ \mathrm{nm}) \quad (12)$$

This photolysis pathway terminates the cycle and reduces the $HO_x$ yield. In the case of the cycle initiated by $O(^1D) + CH_4$, only two $HO_x$ are produced.

Recent studies[3−6] have also indicated that convectively injected acetone [$(CH_3)_2CO$], hydrogen peroxide ($H_2O_2$), methyl hydroperoxide ($CH_3OOH$), and HCHO can be significant secondary sources of $HO_x$ in the upper troposphere. Wennberg et al. report the measured concentrations of OH and $HO_2$ in the middle/upper troposphere to be significantly larger than would be expected on the basis of production from $O_3$, $H_2O$, and $CH_4$ alone.[7] Inclusion of production of $HO_x$ from the photolysis of acetone brought their model to a much better agreement with observed [$HO_x$]:

$$(\mathrm{CH_3})_2\mathrm{CO} + h\nu \rightarrow \mathrm{CH_3CO} + \mathrm{CH_3} \qquad (13)$$

$$\mathrm{CH_3CO} + \mathrm{O_2} + \mathrm{M} \rightarrow \mathrm{CH_3C(O)O_2} + \mathrm{M} \qquad (14)$$

$$\mathrm{CH_3C(O)O_2} + \mathrm{NO} \rightarrow \mathrm{CH_3} + \mathrm{CO_2} + \mathrm{NO_2} \qquad (15)$$

where the $CH_3$ produced in reactions 13 and 15 can then proceed through reactions 3−10 to produce $HO_2$. Acetone concentrations were not measured in their study, however, but were estimated from the measured [CO] and correlation of these species from a previous field campaign.[8]

Formaldehyde is the principal intermediate in the oxidation of acetone and $CH_3OOH$, as well as all other hydrocarbons, in the troposphere as seen in reaction 7. In situ measurements of HCHO are important in quantifying the contributions of hydrocarbons to the production of $HO_x$ in the upper troposphere, especially in the absence of fast, precise, and accurate measurements of acetone and peroxides. Currently, several detection techniques are employed in continuous in situ HCHO instruments: tunable diode laser absorption spectroscopy,[9] coil/2,4-dinitrophenylhydrazine,[10] 1,3-cyclohexanedione-diffusion scrubber,[11] and the coil enzyme method.[12] The detection limits for these techniques are typically between 10 and 100 pptv achieved in 1 to 5 min of integration. These detection limits, however, are oftentimes higher than HCHO concentrations in the upper troposphere. To fully characterize such regimes with low HCHO levels, instruments with sensitivities in the sub-10 pptv range would be required. Laser-induced fluorescence (LIF) has the potential to provide the high sensitivity and the short response time needed to resolve the interesting spatial and temporal distributions of HCHO.

Many measurements of HCHO absorption cross sections have been made over the years under a wide range of different experimental parameters: spectral range, resolution, temperature, pressure, and method of HCHO generation.[13−20] Prior to this work very few rotationally resolved spectra of HCHO were available: Staak et al. reported the absorption spectrum from 6547 to 6804 $cm^{-1}$ (1468−1527 nm) at 0.001 $cm^{-1}$ resolution,[19] and Pope et al. reported cross sections from 31949−31250 $cm^{-1}$ (313−320 nm) at 0.10 $cm^{-1}$ resolution.[20] Maximizing LIF sensitivity, however, requires narrow lines with large differential cross sections (usually from electronic transitions in the visible-UV) to be matched with narrow line width lasers. The weak absorption lines ($\sigma < 2 \times 10^{-21}$ $cm^2$ $molecule^{-1}$) of HCHO reported by Staak et al.[19] and the significantly lifetime-broadened lines (0.5 $cm^{-1}$ fwhm Lorentzian contribution) reported by Pope et al.[20] are thus unsuitable for HCHO LIF detection. It is important to investigate the structured rotational features of a bound or nondissociative transition in order to identify the optimal LIF excitation wavelength.

Accurate rotationally resolved absolute cross sections of HCHO are also of great importance to the retrieval of precise atmospheric concentrations of HCHO from remote-sensing measurements using satellite and ground based differential optical absorption spectroscopy (DOAS). High-resolution spectra can provide the information needed in identifying an optimal spectral window for the least amount of interference from other atmospheric species. In addition, pressure broadening studies are needed if line shape analysis is to be used in determining HCHO concentrations as a function of altitude. For instance, Chance et al. reported satellite observations of HCHO over North America measured by the Global Ozone Monitoring Experiment (GOME) instrument onboard the ESA ERS-2 satellite.[21] Since reference spectra of trace gases with unique absorption features are used in a multilinear regression to match optical densities in the collected light, it is essential to have accurate absorption cross sections at high resolution and know their temperature and pressure dependences.

This work combines high-resolution, high-wavelength accuracy Fourier transform spectroscopy with a novel, high-accuracy calibration source to provide reliable and accurate measurements of rotationally resolved HCHO cross sections that are essential for the development of in situ HCHO LIF instruments.

## 2. Experimental Methods

**2.1. Apparatus.** Absorption measurements in this study were obtained with a high-resolution Fourier transform spectrometer (Bruker IFS 120HR). The spectrometer has been previously used in this laboratory in studying the 2−0 band of the $A^2\Pi_{3/2} \leftarrow X^2\Pi_{3/2}$ transition in IO and the $A^2\Pi_{3/2} \leftarrow X^2\Pi_{3/2}$ transition of BrO.[22,23] Absorption was measured with use of a xenon lamp source and a silicon UV photodiode detector. An interference filter was placed directly before the detector to limit the amount of stray light reaching the detector. The filter, on occasion, introduced Etalon effects, but since the Etalon features were observed in both the sample and background spectra, they were removed when the absorbance was determined.

Even though Fourier transform spectroscopy provides high-wavenumber precision by referencing the sample interferogram to the zero crossings of the interferogram from a frequency-stabilized helium−neon laser, calibration is still necessary to ensure accuracy. In this study, the absolute wavenumber calibration was done by using the sharp absorption features of iodine in the region 17600−18300 $cm^{-1}$. Twenty isolated and symmetric peaks with normal widths and intensities were identified and referenced to the literature atlas.[24] Low-resolution spectra of HCHO were also used to verify the accuracy of the wavelength scale in the UV by comparing to published spectra.

The experimental apparatus is shown in Figure 1. Gaseous HCHO was introduced into the absorption column by evaporating micron-sized droplets of HCHO/water/methanol solution, produced by a novel microinjector source (discussed in the next section), in a heated glass tube. The microinjector is situated in the center of a showerhead-like carrier gas inlet to prevent wall loss. Dry air with a relative humidity of less than 0.5% was used as the carrier gas, and precise mass flows of the carrier gas were made by using a 200 sccm flow controller (MKS). The temperature reached a maximum in the center of the tube at ∼90 °C with 150 sccm flow of carrier gas, well below the point of thermal dissociation for HCHO.

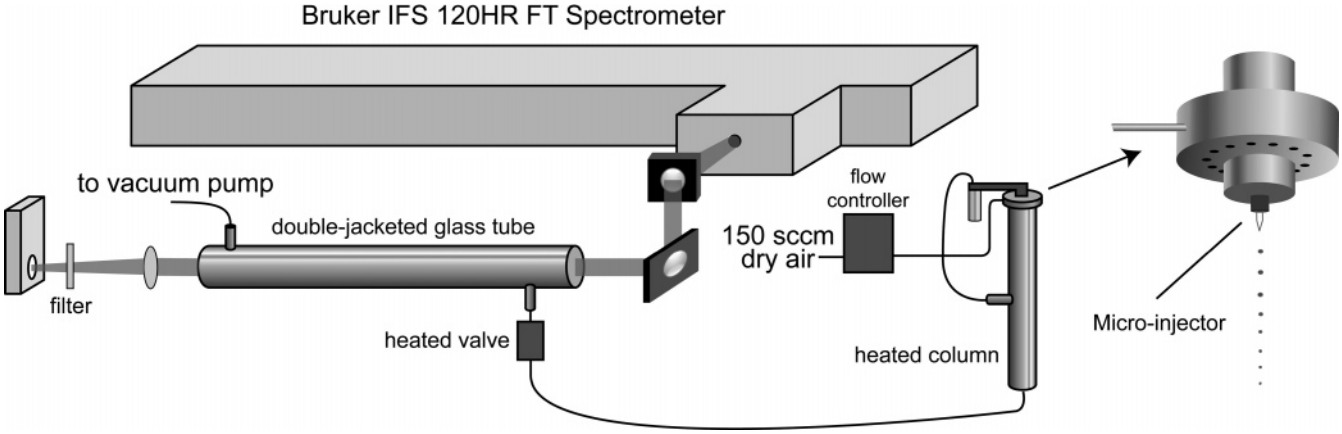


**Figure 1.** A schematic diagram of the experimental apparatus.

A needle valve was placed between the evaporation tube and the absorption column to maintain a pressure differential between the two, a requirement for the operation of the microinjector. The needle valve was heated to approximately 40 °C to prevent any condensation in the valve. The pressure in the heated evaporation tube was kept above 600 Torr for all scans. In addition, the pressure differential between the nozzle and the reservoir of the microinjector was kept at a minimum to prevent the HCHO solution from being sucked into the evaporation tube, and a pressure close to atmosphere was chosen to limit evaporation of the reservoir solution.

A double-jacketed 1-m glass tube with Suprasil windows was used as the absorption column. Spectra were acquired at five different total pressures (75, 150, 225, 300, and 400 Torr) at room temperature, and the pressure measurements were made with capacitance manometer gauges (MKS Baratron). Pressure inside the absorption column was varied by adjusting a valve before the vacuum pump, and constant pressure in the evaporation tube was achieved by compensating the change in pumping speed with the needle valve throughput. A spectrum at 220 K was also obtained at 400 Torr. Low temperatures were achieved by flowing chilled methanol through the outer jacket of the column. The temperature was monitored with a thermistor at the center of the gas flow under the same conditions as the sample scans, and the thermistor was removed from the gas flow during scans.

The experimental procedure was to first obtain a background spectrum with all gases flowing, but with the microinjector off, and then to obtain a sample spectrum of HCHO. The background spectrum was obtained at 0.68 $cm^{-1}$ resolution, much lower than the 0.027 $cm^{-1}$ resolution of the sample spectrum. Since all of the Etalon and filter features are substantially broader than 1 $cm^{-1}$, interpolation of the low-resolution background spectra to match our sample spectra did not pose a problem. A typical background spectrum included 35−40 scans and took about 2 min to obtain while a typical sample spectrum consists of 55−60 scans and required an hour to acquire. A background spectrum was taken after each 1-h sample scan to determine the effects of the Xe lamp output drift. Small variations of the Xe lamp intensity were still observed from scan to scan. To correct for this, the baseline of the high-resolution spectra was adjusted (by no more than 1%) to yield the same integrated cross section as the low-resolution HCHO spectra. The low-resolution studies in this work, however, did not require a baseline offset due to the quickness of each scan. Approximately 1000 sample scans were acquired and averaged to produce each of the spectra presented here. Only the $2^0_0 4^1_0$ band was investigated due to signal-to-noise and time constraints. In addition, the rotational lines of the vibrational bands to the blue are broader due to dissociation and would thus be less interesting for LIF.

The spectrometer was maintained at atmospheric pressure and purged with nitrogen during our experiments. However, the spectral wavenumbers are reported as vacuum wavenumbers. The difference between air and vacuum wavenumbers is significant (about 8 $cm^{-1}$ at 28 300 $cm^{-1}$), and thus care needs to be taken when results from different laboratories are compared.

**2.2. Formaldehyde Generation.** Absolute absorption cross sections of HCHO are difficult to obtain because of its tendency to polymerize and adsorb onto walls. Due to this fact, extreme care was taken to improve upon the existing methods to calibrate HCHO concentrations and to run the experiment at low HCHO mixing ratios. Previously, workers have generated HCHO by heating paraformaldehyde and storing it in a static cell. Cantrell et al. heated paraformaldehyde and trapped the monomer at 77 K, storing it before use.[16] Rogers condensed the monomer and purified it by trap-to-trap distillation.[17] Meller and Moortgat used an ethanol−dry ice trap to remove water and used the formaldehyde immediately.[18] In general, pressure measurements were used to determine the amount of HCHO in the cell to subsequently determine the cross sections. To limit the effects of polymerization and wall loss, we utilized a novel microinjector technique to introduce micron-sized droplets of HCHO/water/methanol solution and evaporated the droplets immediately in a continuous flow of carrier gas. As a result, HCHO was always dilute in the gas phase, making condensation and polymerization highly unfavorable.

The microinjector (Microdrop GmbH) is based on technology similar to that used in inkjet printers. A piezo actuator, upon being triggered by electronic pulses, sends short pressure pulses through a glass capillary filled with liquid. The pressure pulses propagate through the liquid, and the liquid is accelerated, reaching velocities of several meters per second. A liquid jet is then formed at the nozzle, but quickly decelerates due to the pressure loss through the nozzle and the expansion of the actuator. By inertia forces and the surface tension of the liquid, a small liquid volume is separated and forms a spherical droplet that typically leaves the nozzle at 2−3 m/s in air. The droplet size depends on the size of the nozzle. The dispenser used in this study produced droplets with a diameter of ∼70 $\mu$m. Reproducibility of the ejected volume (∼180 pL) is very high when all parameters are kept constant. The mass flow rate (grams/hour) of the microinjector was determined by weighing the dispensed volume after an hour of operation. The liquid was trapped in a syringe carefully placed under the nozzle to

limit airflow and evaporation and was weighed immediately. Knowing the HCHO concentrations in solution and the carrier gas flow rates, HCHO concentrations in the gas phase can be determined and used for the cross section determinations.

**2.3. Determining Formaldehyde Concentrations.** Formaldehyde is commercially available in a solution of water at ~38%, and methanol (10−15%) is added as a preservative to prevent HCHO from polymerizing. For this work, the HCHO solution was diluted with chromatography-grade water to the desired concentration, typically ~10−12 wt %, and passed through a 0.5-$\mu$m filter prior to the loading of the microinjector. No other treatments of the HCHO solution were performed or necessary.

The concentration of HCHO in solution was determined by iodometric titration.[25] A similar method was first developed for the determination of glutaraldehyde with very high precision (0.2%).[26] In iodometry, an oxidizing analyte is added to excess $I^-$ to produce iodine, which is then titrated with standard thiosulfate solution. Formaldehyde reacts with triiodide in basic conditions:

$$HCHO + 3OH^- \rightleftarrows HCO_2^- + 2H_2O + 2e^- \quad (16)$$

$$I_3^- + 2e^- \rightleftarrows 3I^- \quad (17)$$

An excess amount of triiodide is added to the HCHO solution and then back-titrated with commercially available standard sodium thiosulfate ($Na_2S_2O_3$) solution in neutral or acidic solution:

$$I_3^- + 2S_2O_3^{2-} \rightleftarrows 3I^- + S_4O_6^{2-} \quad (18)$$

Starch indicator was added immediately before the equivalence point since $I_3^-$ is present throughout the reaction up to the equivalence point. Iodine can remain bound to starch particles even after the equivalence point is reached if starch is added too early. A standard solution of $I_3^-$ was made by adding a weighed quantity of pure potassium iodate ($KIO_3$) to a small excess of potassium iodide. Addition of excess strong acid produces $I_3^-$ by quantitative reverse disproportionation:

$$IO_3^- + 8I^- + 6H^+ \rightleftarrows 3I_3^- + 3H_2O \quad (19)$$

The $I_3^-$ solution was always used immediately to prevent oxidation by air. Typically, the HCHO solution used in this study had a HCHO concentration of ~10−12 wt %.

The accuracy and reliability of using iodometric titrations to determine concentrations of HCHO in solution was cross checked by using the dimedon reagent (5,5-dimethylcyclohexanedione-1,3).[27] By introducing excess dimedon to a HCHO solution in mildly acidic conditions, two molecules of dimedon condense with one molecule of HCHO through loss of a molecule of water. The precipitate was then filtered out, dried overnight in an oven at 60 °C, and weighed to determine the original HCHO concentration. Both techniques agreed within experimental uncertainties of 2%. Iodometric titration was chosen as the primary technique because it is simpler and more rapid. Titrations were performed prior to each experimental run.

The gas-phase HCHO concentrations, $[HCHO]_{gas}$ (units of molecule $cm^{-3}$) were calculated through the following relationship:

$$[HCHO]_{gas} = \frac{X_{HCHO} F_\mu}{F_{carrier} + F_\mu}[M] \quad (20)$$

where $X_{HCHO}$ is the mole fraction of HCHO in solution, $F_\mu$ is the flow rate of the microinjector and $F_{carrier}$ is the carrier gas flow rate (both in units of molecule $s^{-1}$), and [M] is the concentration of all gaseous molecules determined by the experimental pressure (units of molecule $cm^{-3}$).

Typical HCHO mixing ratios in the gas phase with a 75-Hz injector repetition rate, 70-$\mu$m diameter droplets, 12% HCHO solution (by weight), and 150-sccm carrier gas flow are less than 400 ppm, which correspond to HCHO partial pressures of less than 100 mTorr. Low mixing ratios and a dynamic flow cell were chosen to limit the effects of wall loss and polymerization and to prevent deviations from the linear behavior of the Beer−Lambert law.

The overall uncertainty in the reported absorption cross sections depends on the uncertainties in the measured optical path length, temperature, pressure, $X_{HCHO}$, $F_\mu$, $F_{carrier}$, and absorbance. The optical path length can be measured to better than 0.5%. The uncertainties of the temperature measurements are 0.7% (±2 K) at room temperature and 2% (±5 K) at low temperatures. The quoted uncertainties in the pressure measurements were <0.15%, while the flow rate measurements are expected to have an uncertainty of <0.1%. Determination of the HCHO concentration in solution by titration has a reported accuracy of 0.2%,[26] and together with the other measurements results in an uncertainty of ~1% for $[HCHO]_{gas}$. From the background spectra, it was determined that the baseline fluctuations were <0.1%, corresponding to a 3% root-mean-square accuracy of the absorbance measurements. Including the uncertainty from the baseline offset for the high-resolution spectra (<1%), the overall uncertainty for the absorption cross sections is estimated to be no greater than ±5%.

## 3. Results

**3.1. Absorption Cross Sections at 298 K.** Before measuring HCHO cross sections, several experiments were done to investigate the possible interference from water or methanol, the effects of wall loss and/or polymerization of HCHO, and the properties of the microinjector to determine the optimal experimental conditions for the measurements. Spectra of blank solutions of water and methanol were measured, and no absorption features were observed in the 351−356 nm spectral window. In another experiment, the absorption column was filled to 500 Torr with a few hundred ppm of HCHO in dry air with the vacuum pump isolated. Low-resolution spectra of the trapped mixture were then acquired at 15-min intervals. No noticeable loss of HCHO was observed even after several hours. Since the residence time is only several minutes in our normal flow conditions, loss of HCHO in the absorption column was determined to be unimportant with our experimental conditions.

Experiments were also performed to investigate the linearity of the microinjector and whether all of the dispensed microdroplets were evaporated. The microinjector was triggered with an external function generator. The repetition rate was varied in the range from 50 to 250 Hz, and a linear dependence of observed HCHO concentration vs repetition rate was observed between 50 and 150 Hz. In the higher repetition rate limit, lower HCHO concentrations were observed due to the incomplete evaporation of the microdroplets; droplets can be visibly seen reaching the bottom of the evaporation tube at high, but not low, repetition rates. Operating microinjector repetition rates were thus chosen to be within the linear range, typically at 75 Hz.

Absorption cross sections were calculated by using the napierian (base e) absorbances at each wavenumber through the

relationship:

$$\sigma(\tilde{\nu}) = \frac{\ln[I_o(\tilde{\nu})/I(\tilde{\nu})]}{l\,[\mathrm{HCHO}]_{gas}} \tag{21}$$

where $\sigma(\tilde{\nu})$ is the absorption cross section (in units of $cm^2$ $molecule^{-1}$), $I_o(\tilde{\nu})$ and $I(\tilde{\nu})$ are the spectral intensities at the wavenumber $\tilde{\nu}$ with the microinjector off and on, respectively, $l$ is the optical path length (in cm), and $[HCHO]_{gas}$ is the gas-phase concentration of HCHO (in units of molecule $cm^{-3}$).

Formaldehyde absorbs ultraviolet radiation in the spectral range 260−360 nm, with the $S_1 \leftarrow S_0$ electronic transition giving rise to the $A^1A_2-X^1A_1$ band system.[28] The first strong band in the absorption spectrum is the vibronically allowed $4^1_0$ band, which forms the first member of a progression involving several quanta of the CO stretching vibration. In Figure 2, the full $2^0_04^1_0$ rotationally resolved vibrational band of the $A^1A_2-X^1A_1$ electronic transition of HCHO in the spectral range of 28130−28430 $cm^{-1}$ at 298 K and 225 Torr at an apodized resolution of 0.027 $cm^{-1}$ is shown and compared to a 0.68 $cm^{-1}$ resolution spectrum obtained in this study. The strongest absorption lines ($\sigma > 1.3 \times 10^{-19}$ $cm^2$ $molecule^{-1}$) of the $2^0_04^1_0$ band at 298 and 220 K are also given in Table 1. From those, symmetric and isolated lines that may be suitable for LIF excitation are identified. It should be mentioned at this point that the reported resolutions in this study are the instrument line widths that take the apodization functions into account. Due to the need for high resolution, the boxcar function, a weak apodization function, was chosen.

**3.2. Comparison of the Low-Resolution 298 K Spectrum with Previous Measurements.** Comparisons were made with previous measurements of the absorption cross sections of HCHO at lower resolutions. This was a critical test to confirm the validity of the calibration technique. In Figure 3 a portion of the low-resolution spectra obtained in this work is shown with the spectra of Cantrell et al.[16] and Meller and Moortgat.[18] The low-resolution spectrum of this study was acquired at a resolution of 0.68 $cm^{-1}$ and subsequently binned and averaged to 1 and 2 $cm^{-1}$. It can be seen that the spectra obtained in this work are slightly noisier. This is due to the fact that our measurements were made at a higher resolution, which is intrinsically noisier and requires longer scan times (giving fewer samples to average). In addition, higher noise was expected because of the substantially lower HCHO concentration, and thus absorbances, of this work. It is important to notice that the work done by Cantrell et al.[16] reports vacuum wavenumbers

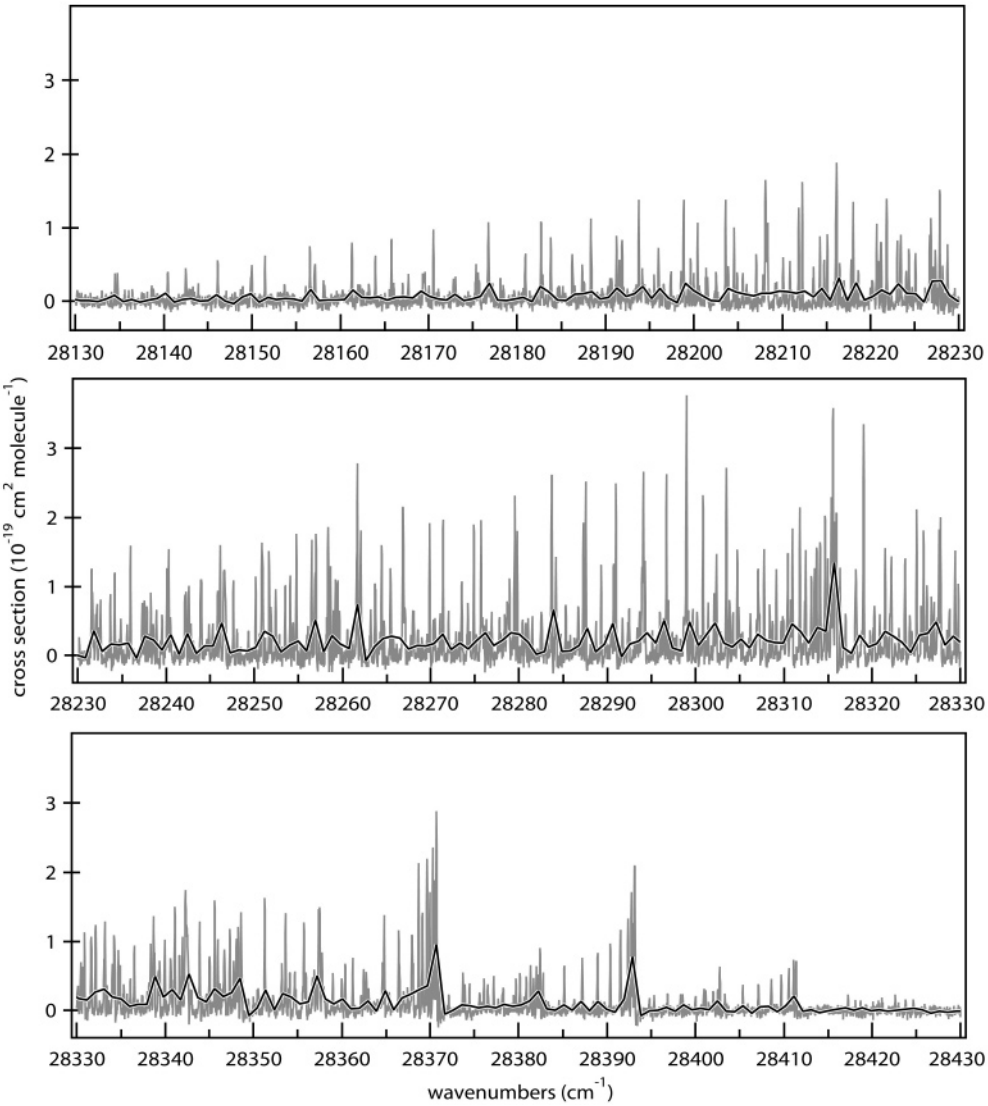


**Figure 2.** UV absorption cross sections of the $2^0_04^1_0$ vibrational band of the $A^1A_2-X^1A_1$ electronic transition of HCHO at 298 K in the range 28130−28430 $cm^{-1}$. The rotationally resolved spectrum (gray) was acquired at 0.027 $cm^{-1}$ and 225 Torr, the lower resolution spectrum (black) at 0.68 $cm^{-1}$ and 500 Torr.

**TABLE 1: Peak Differential Cross Sections of the Strongest HCHO Absorption Lines ($\sigma > 1.3 \times 10^{-19}$ cm$^2$ molecule$^{-1}$ at 400 Torr) of the $2^0_0 4^1_0$ Band at 298 and 220 K[a]**

| | $\sigma$, $10^{-19}$ cm$^2$ molecule$^{-1}$ | | | $\sigma$, $10^{-19}$ cm$^2$ molecule$^{-1}$ | |
|---|---|---|---|---|---|
| wavenumbers | 220 K | 298 K | wavenumbers | 220 K | 298 K |
| 28 246.62 | 1.54 | 1.04 | 28 302.30 | 1.39 | 0.85 |
| 28 250.87[b] | 1.37 | 1.16 | 28 303.45[b] | 1.72 | 1.57 |
| 28 261.66[b] | 2.00 | 1.62 | 28 311.80[b] | 1.50 | 1.22 |
| 28 266.87[b] | 1.68 | 1.41 | 28 315.50 | 2.48 | 2.15 |
| 28 275.73 | 1.37 | 1.15 | 28 315.89 | 2.58 | 1.66 |
| 28 279.52 | 1.18 | 1.32 | 28 319.03[b] | 2.26 | 1.88 |
| 28 283.68[b] | 2.11 | 1.75 | 28 327.59 | 1.63 | 1.24 |
| 28 287.54 | 1.72 | 1.49 | 28 327.77 | 1.66 | 1.29 |
| 28 291.01 | 1.76 | 1.44 | 28 342.35 | 1.64 | 1.34 |
| 28 293.99 | 2.04 | 1.74 | 28 357.48 | 1.37 | 1.05 |
| 28 296.70 | 1.87 | 1.48 | 28 368.69[b] | 1.44 | 1.30 |
| 28 298.93[b] | 2.60 | 2.09 | 28 369.62 | 1.46 | 1.24 |
| 28 300.83[b] | 1.86 | 1.26 | 28 370.31 | 1.51 | 1.45 |
| 28 246.62 | 1.54 | 1.04 | 28 370.49 | 1.47 | 1.28 |
| 28 250.87 | 1.37 | 1.16 | | | |

[a] Experimental uncertainties are ±5% (1 $\sigma$). [b] Isolated absorption lines that may be suitable for LIF excitation.

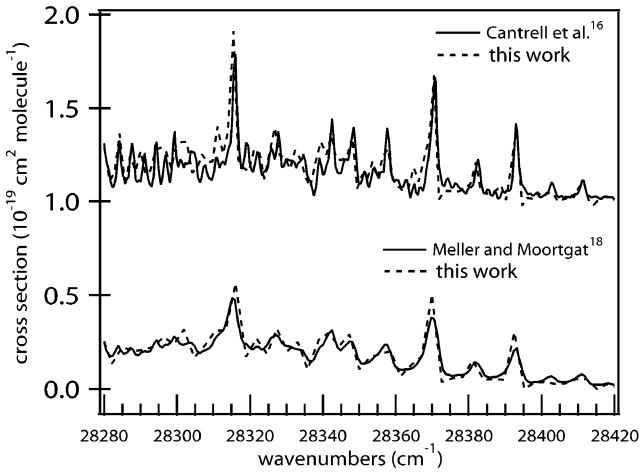


**Figure 3.** Comparison of the low-resolution cross sections with earlier studies in the range 28280−28420 cm$^{-1}$ at 1 and 2 cm$^{-1}$ resolution. The 1 cm$^{-1}$ resolution spectra from this work and Cantrell et al.[16] are offset by $1 \times 10^{-19}$ cm$^2$ molecule$^{-1}$ for clarity.

**TABLE 2: Integrated Absorption Cross Sections for the $2^0_0 4^1_0$ Band Over the Wavenumber Range 28130−28430 cm$^{-1}$ at Room Temperature**

| | integrated absorption cross sections, $\times 10^{-18}$ cm$^2$ molecule$^{-1}$ cm$^{-1}$ |
|---|---|
| this work | 4.11 |
| Meller and Moortgat[18] | 4.24 |
| Cantrell et al.[16] | 3.67 |

and that of Meller and Moortgat[18] reports air wavenumbers, and the difference is large (8 cm$^{-1}$ at 28 320 cm$^{-1}$). Corrections to the air wavenumbers were made accordingly by accounting for the refractive index of air, and all spectra are presented here in vacuum wavenumbers.

The integrated cross sections of our low-resolution spectra and those of previous works were computed by using a trapezoidal integration and are shown in Table 2. It can be seen that the cross sections obtained in this study are in excellent agreement with Meller and Moortgat,[18] the highest cross sections of all measurements in the 290−355 nm range.[13,14] Since HCHO adsorption onto the cell walls or polymerization, believed unimportant in this work, would result in systematically low values for the absorption cross sections and the strong absorption

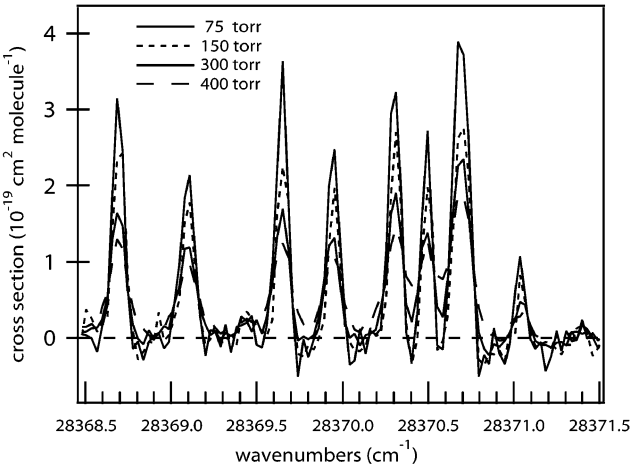


**Figure 4.** The 0.027 cm$^{-1}$ resolution absorption cross sections of HCHO at 75, 150, 300, and 400 Torr at 298 K in the range 28368.5−28371.5 cm$^{-1}$.

peaks in this spectral region are expected to have a nonlinear Beer−Lambert behavior, it is critical to measure at very low optical thickness. The HCHO concentrations used in this work never exceeded 400 ppm at all pressures while Cantrell et al.[16] operated at a few percent of HCHO (10 Torr of HCHO in 500 Torr of $N_2$) and Meller and Moortgat[18] did not use a bath gas but operated at very low HCHO partial pressures (500 mTorr). The excellent agreement of the cross sections obtained in this work with those of Meller and Moortgat,[18] despite using very different HCHO generation methods, may suggest that operating at low HCHO mixing ratios or partial pressures is paramount to achieve reliable cross section measurements.

**3.3. Pressure Dependence of Absorption Cross Sections.** The rotationally resolved absorption cross sections of HCHO were also measured at various pressures between 75 and 400 Torr at 298 K and 0.027 cm$^{-1}$ resolution. The spectra at the four pressures 75, 150, 300, and 400 Torr are displayed in Figure 4 for the range from 28368.5 to 28371.5 cm$^{-1}$. This spectral window was chosen for the sake of clarity in the plot, and data are available for the entire $2^0_0 4^1_0$ band in digital form. The integrated cross sections over the entire band are the same at all pressures as one would expect. It can be seen in Figure 4 that the rotational lines of HCHO have a strong pressure dependence.

Pressure broadening of the lines at 28 188.37, 28 319.03, 28 351.27, and 28 390.38 cm$^{-1}$ in dry air (1−5% relative humidity from the evaporated water) was studied. The absorption lines were fitted to a Voigt profile, and from the Voigt fits the Gaussian and Lorentzian contributions to the overall width were determined. At the low-pressure limit of 75 and 150 Torr, the observed line widths were entirely dominated by Doppler broadening. An asymptotic Gaussian width of 0.07 cm$^{-1}$ was obtained, in good agreement with the width calculated for the ambient temperature within the uncertainties of the fit and measurement. The Lorentzian pressure broadening contribution to the line width increased linearly with pressure at pressures >150 Torr where Doppler broadening was not dominant. With a linear regression of the Lorentzian widths versus pressure, an average pressure broadening coefficient of the HCHO lines was determined to be $1.8 \times 10^{-4}$ cm$^{-1}$ Torr$^{-1}$.

Pope et al. incorporated a 0.5 cm$^{-1}$ fwhm Lorentzian contribution to the line shape of their simulations to account for lifetime broadening of the $2^3_0 4^1_0$ and $2^2_0 4^3_0$ bands.[20] From the measurements of this work, however, contributions to the line widths from lifetime broadening were demonstrated to be

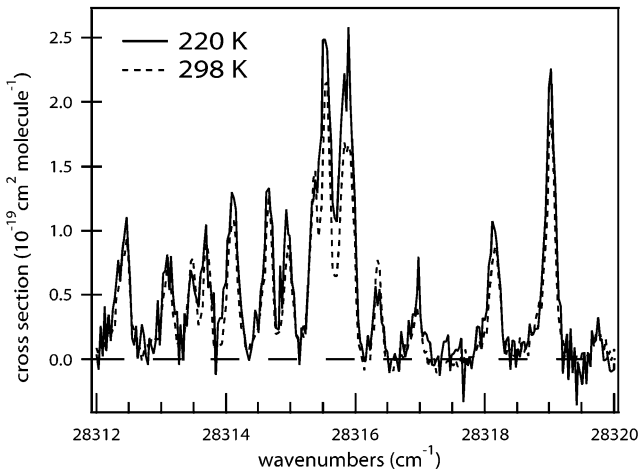


**Figure 5.** The 0.027 cm$^{-1}$ resolution absorption cross sections of HCHO at 298 and 220 K at 400 Torr in the range 28312−28320 cm$^{-1}$.

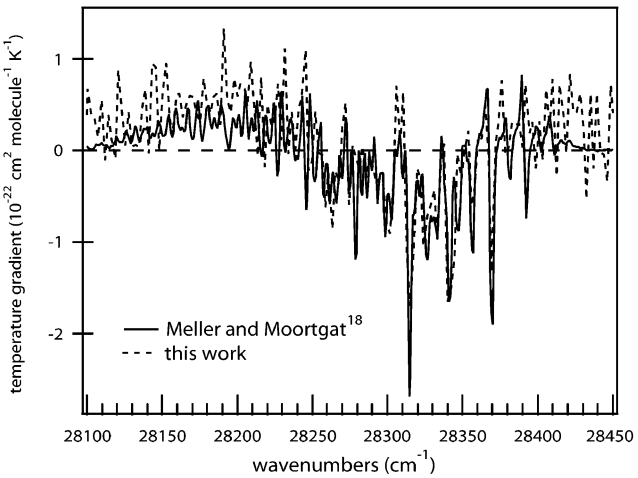


**Figure 6.** Comparison of temperature gradients of HCHO in the range 28100−28450 cm$^{-1}$. The result from this work was reduced to a resolution of 2 cm$^{-1}$ from 0.027 cm$^{-1}$ by averaging.

insignificant for the $2^0_0 4^1_0$ band. The fact that the lines in the $2^0_0 4^1_0$ band are not substantially lifetime broadened reinforces the evidence that rotational lines of this vibrational band can be an ideal choice for the LIF excitation wavelength.

**3.4. Temperature Dependence of Absorption Cross Sections.** Absorption spectra of HCHO were also acquired at 220 K over the entire $2^0_0 4^1_0$ band at 0.027-cm$^{-1}$ resolution. Because of the high mixing ratio of water from the evaporation of the HCHO solution in our flow, condensation was inevitable and substantial. As a result, absolute cross sections at 220 K could not be determined quantitatively. To correct for condensation, the 220 K spectra were scaled with a multiplicative factor so that the integrated cross section over the entire band was equal to that at room temperature. This is believed to be acceptable because even if fewer excited rotational states are populated at 220 K, the overall population should stay the same. The spectra at 298 and 220 K are shown in Figure 5 for the range 28312−28320 cm$^{-1}$. Again, only a small portion of the spectra is shown for clarity. It can be seen that the amount of temperature dependence of the rotational lines varies differently from peak to peak, in agreement with the theory that the distribution of rotational−vibrational states changes with temperature. Increases in the intensities of the absorption lines at 220 K from those at 298 K suggest that those peaks correspond to transitions from lower rotational states.

A temperature gradient $\Gamma(\tilde{\nu})$ was calculated for 2-cm$^{-1}$ intervals from the 0.027-cm$^{-1}$ resolution spectra measured at 298 and 220 K. $\Gamma(\tilde{\nu})$ is defined by the following equation:

$$\sigma(\tilde{\nu},T) = \sigma(\tilde{\nu},298\text{K}) + \Gamma(\tilde{\nu})(T - 298\text{ K}) \qquad (22)$$

where $\sigma(\tilde{\nu},T)$ is the absorption cross section of HCHO at the wavenumber $\tilde{\nu}$ and temperature $T$. The temperature gradient is displayed in Figure 6 and compared to the results from Meller and Moortgat[18] at the same resolution. Excellent agreement can be seen between the two results. The temperature gradient from this work is slightly noisier, but that should be expected because of the averaging of the higher resolution, noisier spectra of this work.

## 4. Conclusions

Rotationally resolved UV absorption cross sections of HCHO have been measured as a function of pressure and temperature over a wide range of values for the wavenunber range 28100−28500 cm$^{-1}$. Results from this work provide rotational resolution of the $2^0_0 4^1_0$ vibrational band of the $A^1A_2-X^1A_1$ electronic transition of HCHO. The measured cross sections over this band are ∼10% greater than earlier recommended values of Cantrell et al.[16] but are in excellent agreement with those of Meller and Moortgat.[18] With the development of in situ HCHO LIF instruments in mind, several potential absorption lines, e.g., one at 28 319.03 cm$^{-1}$ (353.119 nm), were identified. The peaks' strong differential cross sections of $3-6 \times 10^{-19}$ cm$^2$ molecule$^{-1}$ at 75 Torr, isolation from neighboring lines, and wavelength accessibility with a readily available Nd:YAG-pumped Ti:Sapphire or dye laser make them ideal candidates for the LIF excitation wavelength. Prior to this work, these narrow features have never been reported in this spectral region where the effects of lifetime broadening are small. With the results of the pressure-broadening and low-temperature studies of this work, development of instruments for high-sensitivity, in situ measurements of HCHO is now underway.

The low-resolution studies of this work also successfully demonstrated that the microinjector technique can be used as a reliable and invaluable calibration method for nonvolatile, "sticky" species that have been traditionally difficult to study quantitatively in the gas phase, such as sulfuric acid.[29] The microinjector has also been used in this laboratory for the calibration of evaporation-dependent processes such as the fractionation of isotopic water.[30]

The data from this work can be obtained in digital form from the authors (co@huarp.harvard.edu). These data sets contain the absorption cross sections of HCHO acquired in this study at 75, 150, 225, 300, and 400 Torr at 298 K and 400 Torr at 220 K at 0.027 cm$^{-1}$ apodized resolution in the spectral range 28100−28500 cm$^{-1}$ (351−356 nm).

**Acknowledgment.** We gratefully acknowledge Geert K. Moortgat and Chris A. Cantrell for granting us permission to include their work and for providing their data in digital form. Rob Stanhope is thanked for his extensive help on the graphics. D.T.C. acknowledges support from the National Science Foundation Graduate Research Fellowship Program.

## References and Notes

(1) Logan, J. A.; Prather, M. J.; Wolfsy, S. C.; McElroy, M. B. *J. Geophys. Res*. **1981**, *86*, 7210.

(2) Moortgat, G. K.; Seiler, W.; Warneck P. *J. Chem. Phys*. **1983**, *78*, 1185.

(3) Singh, H. B.; Kanakidou, M.; Crutzen, P. J.; Jacob, D. J. *Nature* **1995**, *378*, 50.

(4) Prather, M. J.; Jacob, M. J. *Geophys. Res. Lett*. **1997**, *24*, 3189.

(5) Jaegle, L.; et al. *Geophys. Res. Lett*. **1997**, *24*, 3181.
(6) Jaegle, L.; Jacob, D. J.; Brune, W. H.; Tan, D.; Faloona,, I. C.; Weinheimer, A. J.; Ridley, B. A.; Campos, T. L.; Sachse, G. W. *Geophys. Res. Lett*. **1998**, *25*, 1709.
(7) Wennberg, P. O.; et al. *Science* **1998**, *279*, 49.
(8) Singh, H. B.; Ohara, D.; Herlth, D.; Sachse, W.; Blake, D. R.; Bradshaw, J. D.; Kanakidou, M.; Crutzen, P. J. *J. Geophys. Res.* **1994**, *99*, 1805.
(9) Wert, B. P.; Fried, A.; Rauenbuehler, S.; Walega, J.; Henry, B. *J. Geophys. Res*. **2003**, *108*, 4350.
(10) Lee, Y.-N.; Zhou, X.; Leaitch, W. R.; Banic, C. M. *J. Geophys. Res*. **1996**, *101*, 29,075.
(11) Fan, Q.; Dasgupta, P. K. *Anal. Chem*. **1994**, *66*, 551.
(12) Heikes, B.; et al. *J. Geophys. Res*. **1996**, *101*, 14,741.
(13) McQuigg, R. D.; Calvert, J. G. *J. Am. Chem. Soc*. **1969**, *91*, 1590.
(14) Bass, A. M.; Glasgow, L. C.; Miller, C.; Jesson, J. P.; Filkin, D. L. *Planet. Space Sci*. **1980**, *28*, 675.
(15) Moortgat, G. K.; Kippel, W.; Moebus, K. H.; Seiler, W.; Warneck, P. FAA Rep. N. FAA-EE-80-47, Federal Aviation Administration, 1980, Washington, D.C.
(16) Cantrell, C. A.; Davidson, J. A.; McDaniel, A. H.; Shetter, R. E.; Calvert, J. G. *J. Phys. Chem*. **1990**, *94*, 3902.
(17) Rogers, J. D. *J. Phys. Chem*. **1990**, *94*, 4011.
(18) Meller, R.; Moortgat, G. K. *J. Geophys. Res*. **2000**, *105*, 7089.
(19) Staak, M.; Gash, E. W.; Venables, D. S.; Ruth, A. A. *J. Mol. Spectrosc*. **2005**, *229*, 115.
(20) Pope, F. D.; Smith, C. A.; Ashfold, M. N. R.; Orr-Ewing, A. J. *Phys. Chem. Chem. Phys*. **2005**, *7*, 79.
(21) Chance, K.; Palmer, P. I.; Spurr, R. J. D.; Martin, R. V.; Kurosu, T. P.; Jacob, D. J. *Geophys. Res. Lett*. **2000**, *27*, 3461.
(22) Wennberg, P. O.; Brault, J. W.; Hanisco, T. F.; Salawitch, R. J.; Mount, G. H. *J. Geophys. Res*. **1997**, *102*, 8887.
(23) Wilmouth, D. M.; Hanisco, T. F.; Donahue, N. M.; Anderson, J. G. *J. Phys. Chem. A* **1999**, *103*, 8935.
(24) Gerstenkorn, S.; Luc, P. *Rev. Phys. Appl*. **1979**, *14*, 791.
(25) Harris, D. C. *Quantitative chemical analysis*, 5th ed.; W. H. Freeman and Co.: New York, 1998.
(26) Frigerio, N. A.; Shaw, M. J. *J. Histochem. Cytochem*. **1969**, *17*, 176.
(27) Yoe, J. H.; Reid, L. C. *Ind. Eng. Chem*. **1941**, *13*, 238.
(28) Clouthier, D. J.; Ramsay, D. A. *Rev. Phys. Chem*. **1983**, *34*, 31.
(29) Hintze, P. E.; Kjaergaard, H. G.; Vaida, V.; Burkholder, J. B. *J. Phys. Chem. A* **2003**, *107*, 1112.
(30) St. Clair, J. M.; et al. In preparation.